Study of structural, electrical, and dielectric properties of phosphate-borate glasses and glass-ceramics

Cite as: J. Appl. Phys. **120**, 051701 (2016); https://doi.org/10.1063/1.4958935
Submitted: 30 October 2015 • Accepted: 18 December 2015 • Published Online: 18 July 2016

B. M. G. Melo, M. P. F. Graça, P. R. Prezas, et al.

JOURNAL OF APPLIED PHYSICS **120**, 051701 (2016)

Study of structural, electrical, and dielectric properties of phosphate-borate glasses and glass-ceramics

B. M. G. Melo,[1] M. P. F. Graça,[1,a)] P. R. Prezas,[1] M. A. Valente,[1] A. F. Almeida,[2] F. N. A. Freire,[2] and L. Bih[3]
[1]*Physics Department (I3N), Aveiro University, Campus Universitário de Santiago, Aveiro, Portugal*
[2]*Mechanics Engineering Department, Ceará Federal University, Fortaleza, Brazil*
[3]*Equipe Physico-Chimie la Matière Condensée, Faculté des Sciences de Meknès, Meknès, Morocco*

(Received 30 October 2015; accepted 18 December 2015; published online 18 July 2016)

In this work, phosphate-borate based glasses with molar composition $20.7P_2O_5$–$17.2Nb_2O_5$–$13.8WO_3$–$34.5A_2O$–$13.8B_2O_3$, where A = Li, Na, and K, were prepared by the melt quenching technique. The as-prepared glasses were heat-treated in air at 800 °C for 4 h, which led to the formation of glass-ceramics. These high chemical and thermal stability glasses are good candidates for several applications such as fast ionic conductors, semiconductors, photonic materials, electrolytes, hermetic seals, rare-earth ion host solid lasers, and biomedical materials. The present work endorses the analysis of the electrical conductivity of the as-grown samples, and also the electrical, dielectric, and structural changes established by the heat-treatment process. The structure of the samples was analyzed using X-Ray powder Diffraction (XRD), Raman spectroscopy, and density measurements. Both XRD and Raman analysis confirmed crystals formation through the heat-treatment process. The electrical ac and dc conductivities, σ_{ac} and σ_{dc}, respectively, and impedance spectroscopy measurements as function of the temperature, varying from 200 to 380 K, were investigated for the as-grown and heat-treated samples. The impedance spectroscopy was measured in the frequency range of 100 Hz–1 MHz. *Published by AIP Publishing.*
[http://dx.doi.org/10.1063/1.4958935]

I. INTRODUCTION

Phosphate based glasses display several interesting properties, namely, low melting temperature and high thermal coefficient, and advantageous optical properties when compared with conventional silicate and borate glasses, such as high transparency, low refractive index, low dispersion, and high ultraviolet transmission. This makes phosphate based glasses attractive material for applications such as sealing materials, medical applications, high power laser applications, and solid state electrolytes.[1–3]

The basic building block of these glasses is the phosphate PO_4 tetrahedra, which consists of one of the oxygen atoms doubly bonded with the phosphorous atom. The tetrahedra can link with each other through covalent bridging oxygen and, subsequently, different phosphate anions are formed.[3] These tetrahedra can be appropriately labeled in accordance with the Q^n terminology, in which the index n represents the number of bridging oxygen per tetrahedron. This index n can be 0, 1, 2, or 3, and the corresponding structural units are named orthophosphate, pyrophosphate, metaphosphate, and ultraphosphate, respectively.[4]

Besides the phosphorus pentoxide, the glass system presented in this work contains a second glass network former, B_2O_3. The structure of vitreous boric oxide is formed by a random three-dimensional network of nearly flat BO_3 triangles with a high fraction of six membered boroxol rings.[5,6] However, when network modifiers, like alkali oxides, are added to a borate glass, boron atoms change from triangular to tetrahedral coordination until it reached some critical concentration of BO_4 tetrahedra.[5,6] The association of these BO_3 and BO_4 units promotes the formation of more complex structural groups,[7] composed by the cross-linking of these 3- and 4-fold coordination boron atoms.[5,6]

The formation of glass-ceramics shows, in a technological point of view, important advantages when compared with single crystals and ceramics, due to the fact that the optical, electrical, mechanical, and chemical properties can be controlled/tuned according to the volume fraction of the active crystalline phase dispersed in the vitreous glassy matrix.[8,9] Therefore, the interest in the preparation, characterization, and technological application of glass and glass-ceramics in systems as substitutes of single crystal materials has been increasing in the past years.[8,9] Although the electrical properties of the single crystals are usually better than the glass-ceramic material due to the fact that the amorphous phase has generally a low dielectric constant, since the growth of single crystals are cost expensive, glass-ceramics become an appealing cheaper alternative.[8,9]

In our recent work,[7] the structural, electrical, and dielectric properties of the glassy system $20.7P_2O_5$-$17.2Nb_2O_5$-$13.8WO_3$-34.5A2O-$13.8B_2O_3$, where A = Li, Na, and K, were investigated. The compositions with Na_2O (A-Na) and K_2O (A-K) led to the formation of transparent glasses, while the one containing Li_2O (A-Li) resulted in a glass-ceramic material. The electrical and dielectric analyses showed that the sample A-Li has predominantly ionic conductivity at the entire evaluated temperature range (200–380 K). According to the $\sigma_{electronic}/\sigma_{ionic}$ ratio, the dc conductivity of the A-Na

a)E-mail: mpfg@ua.pt

and A-K samples can also be regarded as purely ionic at room temperature. The dielectric analysis revealed that, for the A-K and A-Na samples, the dielectric constant is almost constant in the evaluated frequency range (100 Hz–1 MHz), while, for the A-Li sample, the increase observed at lower frequencies can be due to charge accumulation effects at the interfaces amorphous matrix-crystalline domains. For the A-Li and A-Na samples, a dielectric relaxation was observed in the dielectric modulus representation, and the relaxation kinetics analysis revealed an Arrhenius dependency with activation energies of 52.5 kJ/mol and 47.7 kJ/mol, respectively.[7]

In the current work, the effects of the heat-treatment in air, at 800 °C during 4 h, on the structural, electrical, and dielectric properties of the glass samples, were analyzed.

II. EXPERIMENT

A. Sample preparation

Functional glasses with molar composition $20.7P_2O_5$-$17.2Nb_2O_5$-$13.8WO_3$-$34.5A_2O$-$13.8B_2O_3$, where A = Li, Na, and K, were prepared by melt quenching technique, using high purity chemicals (>99%) P_2O_5, Nb_2O_5, WO_3, A_2CO_3, and B_2O_3 in powder form. The reagents, in the appropriate amounts, were mixed at 365 rpm for 30 min in a Fritsch Pulverisette 5 agate ball-mixing planetary system, in order to improve the homogeneity of the mixtures.

Afterwards, the mixtures were melted at 1150 °C in alumina crucibles with a closed lid, for about 15 min. After 7 min at 1150 °C, and for each composition, the crucible was manually stirred in order to homogenize the melt. The complete loss of carbonates was confirmed from the Raman results that reported no vibrations related to CO_3^{2-} groups.

The melts were poured into a stainless steel slab, which was immediately introduced into a furnace pre-heated at 300 °C. The samples were then maintained at 300 °C for about 12 h, in order to improve the glasses' mechanical stability by relieving internal stresses.

The as-prepared glasses were, afterwards, heat-treated in air at 800 °C during 4 h, with a heating rate of 5 °C/min. The heat-treatment temperature was chosen in accordance with the differential thermal analysis,[7] which revealed an exothermic peak for the as-grown glasses between 530 and 600 °C.

In this work, the samples will be termed A-Li, for the glass that contains Li_2O, A-Na, for the sample with Na_2O, and A-K for the glass that incorporates K_2O.

B. Structural and morphological characterization

The X-ray diffraction patterns (XRD) were obtained at room temperature on a Philips X'Pert MPD diffractometer (CuKα radiation, $\lambda = 1.54056$ Å) operating at 45 kV, and 40 mA, with a curved graphite monochromator, an automatic divergence slit, a progressive receiving slit, and a flat plane sample holder in a Bragg-Brentano parafocusing configuration. The acquisition was performed using a scan step of 0.02° in 1 s in the 2θ angle range of 10°–60°. The obtained patterns are shown in Figure 1.

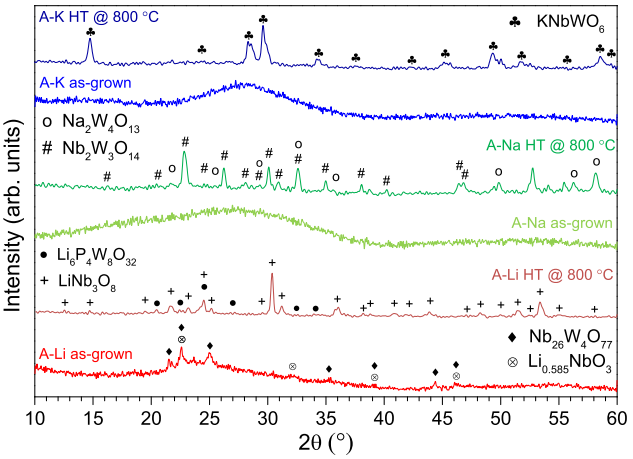

FIG. 1. XRD spectra of the samples.

Room temperature Raman spectroscopy was carried out in a Jobin Yvon HR 800 spectrometer, using the excitation line of 532 nm. The spectra were obtained in a back-scattering geometry, between 100 and 1100 cm^{-1}.

C. Density measurements

The density measurements were realized in an Adam Equipment ADP-110 system, measuring the sample's weight in air and in C_2H_5OH, at 300 K (Archimedes principle). For each sample, the density value was taken as the average of ten measurements. The associated errors are displayed in Figure 3 by the error bars.

D. Electrical and dielectric characterization

The dc electrical conductivity (σ_{dc}) of the samples was measured with a Keithley 617 electrometer, in the temperature range between 200 and 380 K, using a nitrogen bath cryostat setup. During the measurements, the samples were kept in a helium atmosphere to minimize thermal gradients.[13,14]

The ac electrical conductivity (σ_{ac}) and impedance measurements were also performed in the temperature range of 200–380 K, using the same bath cryostat, with a Network Analyzer, Agilent 4294, operating between 100 Hz and 1 MHz in the $C_p - R_p$ configuration (capacitance in parallel with resistance). In both measurements, the temperature of the samples was controlled by an Oxford Research IT-C4. The activation energy (E_a) of the dc and ac conductivities was evaluated in the high temperature range (>285 K), by fitting the data to the Arrhenius law (Equation (1))[10–12]

$$\sigma = \sigma_0 \exp\left(-\frac{E_a}{k_B T}\right), \quad (1)$$

where σ_0 is a pre-exponential factor, E_a is the activation energy, k_B is the Boltzmann constant, and T is the temperature. Using this model, E_a can be calculated from the slope of $ln(\sigma_{dc})$ vs. $1/T$.

The real and complex parts of the permittivity were calculated using the following relations:[10,11]

$$\varepsilon' = \frac{d}{S}\frac{C_p}{\varepsilon_0}, \tag{2}$$

$$\varepsilon'' = \frac{d}{S}\frac{1}{\omega R_p \varepsilon_0}, \tag{3}$$

with C_p being the measured capacitance, R_p the resistance, d the sample thickness, S the electrode area, and ε_0 the vacuum permittivity (8.8542×10^{-12} F/m).

The ac conductivity, σ_{ac}, was calculated using the relation[10–12]

$$\sigma_{ac} = \varepsilon'' \omega \varepsilon_0, \tag{4}$$

where ω is the angular frequency and ε'' is the imaginary part of the complex permittivity.

The polished samples presented flat and parallel faces, with an area close to 3×10^{-5} m^2 and a thickness of about 1 mm. The electrodes, of the analyzed samples, were made by painting the opposite faces of the samples with silver conductive paste.

III. RESULTS AND DISCUSSION

A. Structural characterization

The XRD spectra of the as-grown and heat-treated samples are shown in Figure 1. The XRD showed that for the as-grown samples, only A-Li glass evidenced formation of crystalline particles, $Nb_{26}W_4O_{77}$, with a monoclinic crystalline structure and a secondary crystalline phase $Li_{0.585}NbO_3$ with cubic crystal structure.

After the heat-treatment, the crystalline phases formed in the A-Li glass are $LiNb_3O_8$ (monoclinic) and $Li_6P_4W_8O_{32}$ (monoclinic). The appearance of the $LiNb_3O_8$ phase could indicate that the heat-treatment promoted the rearrangement of the non-stoichiometric $Li_{0.585}NbO_3$ phase found in the as-grown sample, into a new and more stable crystalline phase.[13,14] In fact, long-term stability of non-stoichiometric lithium niobate ($Li_{1-x}NbO_3$) is observed up to 300 °C, only.[14] Besides this rearrangement, the heat-treatment promotes the disappearance of the $Nb_{26}W_4O_{77}$ phase and the formation of a new lithium rich phase ($Li_6P_4W_8O_{32}$).

The A-Na glass heat-treated (HT) showed the formation of $Nb_2W_3O_{14}$ (tetragonal) and $Na_2W_4O_{13}$ (triclinic) phases, while the A-K sample exhibited the formation of a single $KNbWO_6$ crystalline phase with a cubic crystal system.

The $KNbWO_6$ particles have a pyrochlore-type structure which presents useful properties for materials science applications, including ionic conductivity (both cations and anions), electrical conductivity, and magnetic and ferroelectric properties.[15,16] Additionally, materials on the basis of $K\Lambda WO_6$ (Λ—Nb, Sb, and Ta) compounds can be used as catalysts due to their content of transition metals.[15]

Figure 2 shows the Raman spectra of the prepared samples. For the A-(Na, K) as-grown glasses, their network structure is mainly composed by pyrophosphate and orthoborate groups, and also by structural units where niobium acts as a network former or modifier. For the A-Li sample, the spectrum suggests that its network is mostly constituted by pyrophosphate and metaborate groups. A more detailed study of the as-grown samples spectra and vibrational modes can be found in Ref. 7.

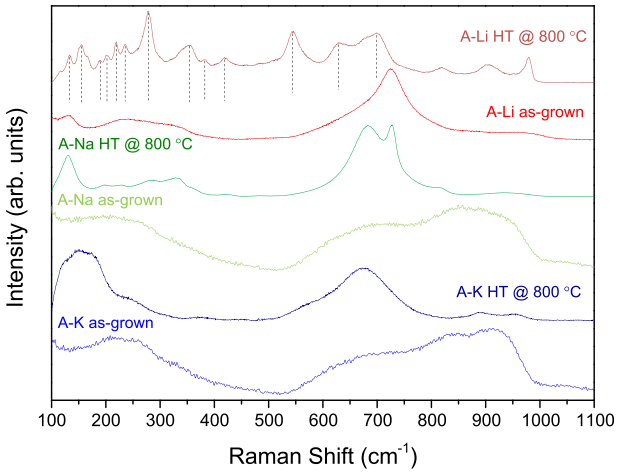

FIG. 2. Raman spectra obtained at room temperature, for the as-grown and heat-treated glasses. The dotted lines in the A-Li heat-treated spectrum display the vibrational modes of $LiNb_3O_8$ particles.

The Raman spectra show that, after the heat-treatment, all samples undergo several structural changes, as could be expected from the XRD observations. For the A-K glass-ceramic, it is observed a broad band between 500 and 800 cm^{-1} where, is centered, at ≅560 cm^{-1}, a smaller band related to υ(W-O) in WO_6 octahedra.[15] However, the biggest contribution of this broad band is given by a band centered at 670 cm^{-1} assigned to υ_s(Nb-O) vibrations in NbO_6[15,17] and/or to υ_s(P-O-P). Besides the stretching modes in WO_6 and NbO_6 octahedra, $KNbWO_6$ crystals can also present stretching modes related to terminal -Nb-O and -W = O bonds,[15] as confirmed by the smaller bands in the 860–960 cm^{-1} region. For lower wavenumbers, bending modes (232 cm^{-1}) of PO_4 tetrahedra[18–20] and vibrations assigned to bending modes of the NbO_6/WO_6 octahedra coupled with translational modes of the potassium ions (156 cm^{-1}) can be found.[15]

According to the XRD results, besides the amorphous matrix, the A-Na glass-ceramic presents a dispersion on its matrix of $Na_2W_4O_{13}$ and $Nb_2W_3O_{14}$ crystalline particles.

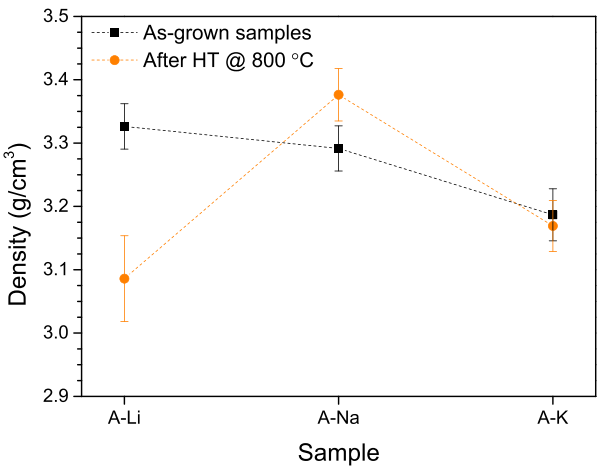

FIG. 3. Density values of the as-grown and heat-treated samples.

Judging on the elements that compose these phases, one can expect the presence of vibrational modes related to WO_6 and NbO_6 structural units. Therefore, the bands between 550 and 750 cm^{-1} can be assigned to vibrations such as υ_s(P-O-P)[21–23] and υ_s(Nb-O) in NbO_6 octahedra[15,17] but also to O-W-O stretching modes.[24] The sharp band at a 726 cm^{-1} could be related to the presence of chain type metaborate groups.[25,26] Finally, the vibrations at lower wavenumbers could be due to bending modes such as δ(O-W-O),[24] δ(O-Nb-O) in NbO_6,[18,20,27] and δ(O-P-O) in PO_4 tetrahedra.[18–20]

For the heat-treated A-Li glass, the Raman spectra show some new bands emerged. XRD analysis showed that the principal crystalline phase is $LiNb_3O_8$. This phase presents a great number of vibrational modes in Raman spectroscopy,[28] and for simplicity, these were identified with dotted lines in the Raman spectra. With this knowledge, it is easy to see that most of the vibrational modes of this sample are in fact assigned to the $LiNb_3O_8$ modes. It is also possible to identify, between 650 and 730 cm^{-1}, a band related to the stretching modes of bridging oxygen in PO_4 tetrahedra.[21–23] The band centered at $\cong$905 cm^{-1} could have possible assignment B-O-B and B-O^- vibrations in orthoborate groups.[26,29,30]

The values of the samples' density are shown in Table I and Figure 3. Although the molar mass of lithium oxide is smaller than that of Na_2O and K_2O, for the as-grown glasses, the sample with highest density is A-Li. This could be related to the crystals formed in this sample which have a structure denser than that of the amorphous matrix, and thus increases the density of this sample.

For the A-Na and A-K as-grown glasses, the XRD analysis showed no crystalline particles formation. Therefore, the smaller density of the A-K glass should be the result of the bulkier structure. This could be related with the increased atomic radius of the potassium ions, and also, given the Raman analysis performed in Ref. 7, with the larger number of orthoborate, orthophosphate, and WO_4 structural units formed in this sample.

According to some studies,[31,32] $Na_2W_4O_{13}$ crystals have a density of 6.3–6.4 g/cm^3 while Mohanty and Fiegel[33] reported a density of 5.51 g/cm^3 for $Nb_2W_3O_{14}$ particles. Therefore, the increase in the density of sample A-Na after heat-treatment can be assigned to the crystallization process, moreover, to the growth of these crystals which have a density greater than the amorphous matrix.

The density of the A-K glass heat-treated is very close to that of the as-grown sample, but for the A-Li glass, the density decreases after the heat-treatment. Since some studies[34] indicate that $LiNb_3O_8$ crystals have a density of 5.03 g/cm^3, the decrease in the density of this sample could be due to the formation of the $Li_6P_4W_8O_{32}$ particles. Alternatively, another possible explanation could be an increase in the porosity resulting from the heat-treatment.

TABLE I. Density values of the prepared samples.

	Density value
A-Li	3.326 ± 0.036
A-Na	3.292 ± 0.036
A-K	3.187 ± 0.041
A-Li HT	3.086 ± 0.068
A-Na HT	3.376 ± 0.041
A-K HT	3.169 ± 0.040

B. Electrical characterization

Table II shows the σ_{dc} values at 300 K and the dc activation energy for the as-grown and heat-treated glasses.

As discussed in our previous work,[7] based on the behavior of the samples' conductivity, for A-(Na, K), two as-grown conduction regimes are present: one in the low temperature range (<250 K) related to electronic conductivity, and the other in the high temperature range assigned to the non-random hopping of the modifier cations.[7,35] For the as-grown A-Li glass, σ_{dc} is predominantly ionic during the entire temperature range of evaluation.

Table II also shows the $\sigma_{electronic}/\sigma_{ionic}$ ratio, which represents the dc conductivity value of each sample at 200 K, divided by σ_{dc} at 300 K. For these samples, at 300 K, their dc conductivity is mainly ionic. While at lower temperatures (200 K) the mobility of the modifier ions is hindered, and some glasses can even have their conductivity predominantly electronic. Therefore, the value of σ_{dc} at 200 K can be used as a reference of the electronic conductivity ($\sigma_{electronic}$). For glasses where the electronic conductivity prevails at lower temperatures, σ_{dc} shows an inflection point and stabilizes to a certain value. This results in a bigger $\sigma_{electronic}/\sigma_{ionic}$ value for those samples. Thus, the determination of this ratio can be an elementary evaluation of the electronic contribution in glasses that exhibit simultaneously ionic and electronic conductivities.

The results of impedance spectroscopy at 300 K and 10 kHz (σ_{ac}, $E_{a\ ac}$, ε', and tan δ) of the samples are presented in Table III.

As for the ac regime, the conductivity of the as-grown glasses[7] does not give a perceptible existence of an inflection point which discerns the presence of two different conduction mechanisms, as observed in the dc regime. Therefore, it is suggested that the ac conductivity should be related to a dipolar mechanism between the modifier ions and the non-bridging oxygen anions in their vicinity.[7,35]

The dc and ac conductivity results of the heat-treated samples are plotted in Figures 4 and 5, respectively. The inset of these figures presents the application of the Arrhenius law in the temperature range of 280–380 K, for the A-Na and A-K heat-treated samples, and between 280 K and 340 K, for

TABLE II. Values of $\sigma_{electronic}/\sigma_{ionic}$, dc conductivity ($\sigma_{dc}$) at 300 K, and dc activation energy ($E_{a\ dc}$) calculated by the Arrhenius equation.

	σ_{dc} (S/m)	$E_{a\ dc}$ (kJ/mol)	$\sigma_{electronic}/\sigma_{ionic}$
A-Li	$4.90 \times 10^{-7} \pm 0.61 \times 10^{-7}$	57.76 ± 0.37	10^{-6}
A-Li HT	$2.93 \times 10^{-8} \pm 0.21 \times 10^{-8}$	53.14 ± 1.63	10^{-5}
A-Na	$2.25 \times 10^{-9} \pm 0.11 \times 10^{-9}$	74.52 ± 0.41	10^{-5}
A-Na HT	$4.78 \times 10^{-9} \pm 0.14 \times 10^{-9}$	63.52 ± 0.12	10^{-3}
A-K	$1.77 \times 10^{-11} \pm 0.16 \times 10^{-11}$	85.61 ± 0.10	10^{-3}
A-K HT	$1.41 \times 10^{-7} \pm 0.07 \times 10^{-7}$	39.69 ± 0.08	10^{-4}

TABLE III. Values of ac conductivity (σ_{ac}), dielectric constant (ε'), and loss tangent ($\tan\delta$) at 300 K and 10 KHz, and ac activation energy ($E_{a\ ac}$) calculated by the Arrhenius equation.

	σ_{ac} (S/m)	$E_{a\ ac}$ (kJ/mol)	ε'	$\tan\delta$ ($\times10^{-2}$)
A-Li	$5.00\times10^{-6}\pm0.19\times10^{-6}$	48.77 ± 0.65	33.89 ± 2.28	26.52 ± 2.06
A-Li HT	$6.73\times10^{-7}\pm0.47\times10^{-7}$	17.74 ± 0.16	26.13 ± 2.72	4.63 ± 0.58
A-Na	$3.22\times10^{-7}\pm0.05\times10^{-7}$	32.65 ± 0.64	15.95 ± 1.33	3.63 ± 0.31
A-Na HT	$8.36\times10^{-7}\pm0.20\times10^{-7}$	31.04 ± 0.67	34.44 ± 2.49	4.36 ± 0.33
A-K	$1.55\times10^{-7}\pm0.03\times10^{-7}$	21.91 ± 0.70	29.46 ± 1.28	0.94 ± 0.04
A-K HT	$2.50\times10^{-5}\pm0.12\times10^{-5}$	23.96 ± 0.09	87.20 ± 7.85	51.46 ± 5.28

the A-Li heat-treated glass, in order to determine the activation energy of the conductivity process at room temperature.

The sample with highest dc conductivity is the A-K treated glass, contrarily to the as-grown case where it was the least conductive sample. From its activation energy (39.69 kJ/mol) and since the conductivity seems to follow a linear evolution with the raise of the temperature, we can conclude that the conductivity is predominantly ionic in this temperature range. The increase of this sample's conductivity is owed to the formation of $KNbWO_6$ particles. These pyrochlore-type structures are built up from corner-sharing WO_6 octahedra, creating networks of hexagonal tunnels.[36,37] Since the univalent cations occupy large framework voids and are weakly linked to its atoms, they can easily migrate along the channels within the structure.[36,37]

For the A-Li treated sample, the same scenario can be observed where the dc conductivity is predominantly ionic. However, for temperatures greater than 340 K, the increment of the conductivity becomes less significant. This observation could suggest that the majority of charge carriers, responsible for the conductivity between 200 K and 340 K, is already activated.

The sample with highest activation energy (63.29 kJ/mol) in the high temperature range is the heat-treated glass A-Na. However, at lower temperatures (<245 K), its activation energy is much smaller (≈4 kJ/mol). Hence, for this range of temperatures, the conductivity can be assigned to electron and/or polaronic hopping between different oxidation states of tungsten (W^{5+} and W^{6+}) and/or niobium (Nb^{4+} and Nb^{5+}) cations.[7] For temperatures above 245 K, the ionic contribution to the total conductivity becomes predominant.

The results of σ_{ac} for the heat-treated samples (Figure 5) show that glass A-K has the highest σ_{ac} during the evaluated temperatures, and that again although both electronic and ionic conductivity coexist, for this sample, the conduction mechanism seems to be ruled by the non-random hopping of the modifier cations.[7,35]

For glass A-Li, at lower temperatures (<230 K), the electronic contribution dominates the conductivity process, as expected,[7] but as the temperature increases, the ac conductivity starts to be governed by the mobility of the mobile ions.

A slightly different behavior can be found for A-Na glass-ceramic, more particularly in its electronic contribution. Contrarily to the other samples, the electronic conductivity dominates for a large range of temperatures (200–300 K). As seen in Figure 5, only for temperatures above 300 K, the ionic conductivity dominates the conductivity process. Although in the remaining glasses the electronic conductivity exhibits

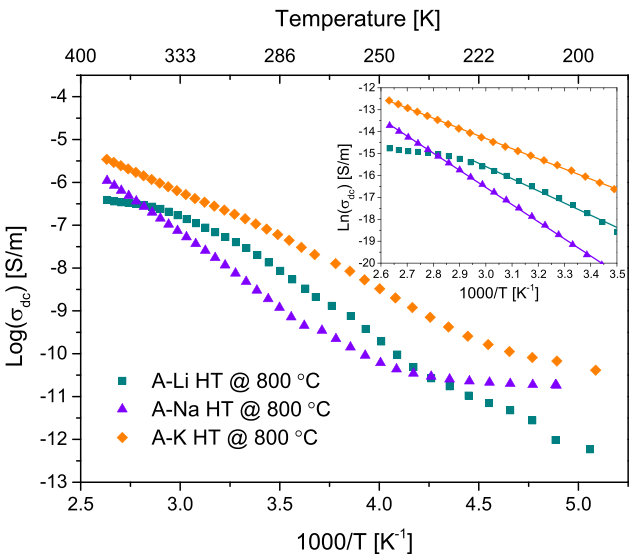

FIG. 4. Dc conductivity (logarithmic scale) versus 1000/T for heat-treated samples (7% is the maximum uncertainty). Linearization of their conductivity using the Arrhenius equation in the graphic inset.

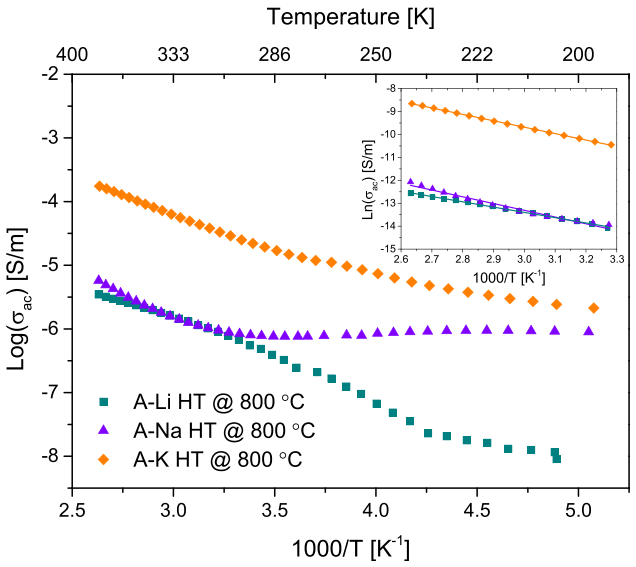

FIG. 5. Ac conductivity (logarithmic scale) versus 1000/T for heat-treated samples (7% is the maximum uncertainty). Linearization of their conductivity using the Arrhenius equation in the graphic inset.

low values, for this sample, its value is around 10^{-6} S/m and proximally stable up to 300 K.

Since the activation energy of A-Na glass-ceramic is smaller in the ac regime, the number of charge carriers able to participate in the conductivity process is larger. This indicates that, in this sample, the electronic conductivity contributes for a wider range of temperatures in the ac regime. Moreover, if we compare its ac conductivity with that of the glass-ceramic A-K, which presents similar values at higher temperatures, one can see that the conductivity at lower temperatures is significantly higher for sample A-Na. This could mean that, for this sample, there is, in fact, a larger number of electrons/polarons available for the conduction process.

In order to evaluate the heat-treatment effect on the electrical and dielectric properties of the samples, an analysis of the samples' activation energy, dc and ac conductivities, dielectric constant, and loss tangent was performed.

The trend of the glasses' dc conductivity and activation energy values (from the high temperature range) shown in Table II can be analyzed in Figure 6. One can see that for the as-grown samples, as expected,[7] the conductivity increases with the increase in the ionic mobility of the alkali cations.

After heat-treatment, the activation energy of glass-ceramic A-Li suffers a small decrease, but its conductivity does not increase. Instead, σ_{dc} decreases one order of magnitude which is most likely due to the growth of $LiNb_3O_8$ and $Li_6P_4W_8O_{32}$ particles. With the formation of these crystalline phases, the number of charge carriers that can diffuse freely through the glass network is diminished.

For sample A-Na, one can see that $E_{a\ dc}$ also decreases after heat-treatment and that its conductivity is lightly favored. The formation of $Na_2W_4O_{13}$ crystals also implies a decreased number of mobile ions that can participate in the conductivity, but nevertheless, the principal crystalline phase is $Nb_2W_3O_{14}$ which has a Tetragonal Tungsten Bronze (TTB) type structure.[38] These types of phases can have high electrical conductivity, which has been attributed to the presence of W^{5+} states.[38] The creation of a large number of W^{5+}-O-W^{6+} bonds promotes an increment of the electronic conductivity. This could be the reason for the increased conductivity after heat-treatment and also for the increased electronic contribution in the ac conductivity of glass-ceramic A-Na.

However, as previously discussed, glass A-K presents the most meaningful changes in the dc conductivity as result of the heat-treatment. $E_{a\ dc}$ reduces from 85.61 to 39.69 (kJ/mol), and the conductivity increases 4 orders of magnitude. This allows to suggest that the formation of $KNbWO_6$ particles in the glass structure improves and increases the dc conductivity of the sample.

The study of Kar and Choudhary[16] concerned ceramics prepared by the solid-state reaction technique achieving $KNbWO_6$ ceramics with $\sigma_{dc} = 1.74 \times 10^{-8}$ (S/m) at 300 K. In comparison, the obtained value of $\sigma_{dc} = 1.41 \times 10^{-7}$ (S/m) for the A-K treated glass is about 10 times bigger.

According to Chernaya *et al.*,[37] $RbNbWO_6$ and $TlNbWO_6$ particles which also have pyrochlore-type structure exhibit electrical polarity for temperatures below 330 and 360 K, respectively, and undergo a phase transition of the ferroelectric-superionic conductor type upon heating. This indicates that these types of crystals present a significantly higher spontaneous polarization in the low-temperature ferroelectric phase and higher ionic conductivity in the high-temperature superionic state.[36,37] Therefore, further experiments in a higher range of temperatures must be done to acquire additional knowledge about its electrical behavior.

The tendency of the glasses' ac conductivity and activation energy values presented in Table III can be seen in Figure 7. The decrease of $E_{a\ ac}$ observed for the as-grown glasses is not followed by an increase of the samples' conductivity. This was discussed in more details in Ref. 7 and is related to the number of charge carriers available.

For the heat-treated A-Li glass, $E_{a\ ac}$ decreases significantly, when compared with the others samples' energy. However, analogously to what was previously discussed for Figure 6, its conductivity also decreases, indicating a significant decrease in the charge carriers' number. After heat-treatment, sample A-Na exhibits again a decrease of the activation energy combined with an increase of σ_{ac}. Similarly to the dc evaluation, for glass-ceramic A-K, σ_{ac} increases significantly even though for this frequency of analysis (10 KHz) its activation energy experiences a small increase.

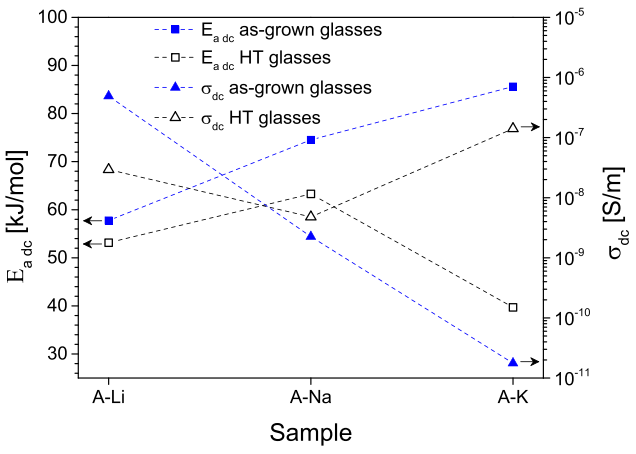

FIG. 6. Evaluation of the dc conductivity (at 300 K) and activation energy of the samples.

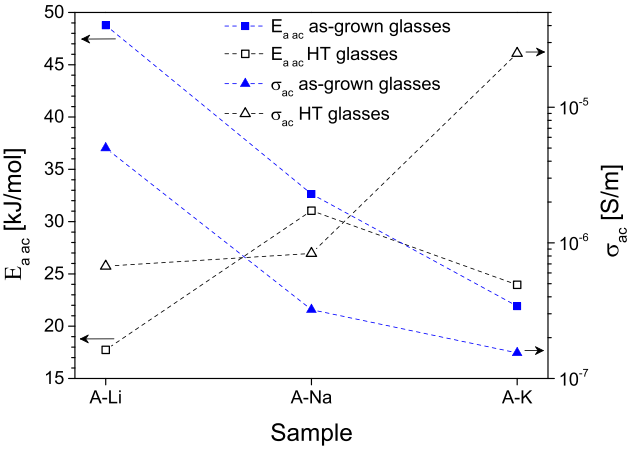

FIG. 7. Evaluation of the ac conductivity (at 10 kHz and 300 K) and activation energy (for a fixed frequency of 10 KHz) of the samples.

These evaluation showed that after the heat-treatment, sample A-K presents the highest electronic ac and dc conductivity values, which makes this sample the most appealing for applications such as electrolytes.

Figure 8 shows the dielectric constant (ε') dependency with the frequency, at 300 K, for the heat-treated samples. It can be observed that for the A-Li and A-Na samples, ε' is practically independent of the frequency and ranges from 20 to 30.

Whereas for sample A-K, which presents a higher value, the dielectric constant increases significantly for lower frequencies. This last behavior should be assigned to charge accumulation effects at the interfaces amorphous matrix-crystalline structural units.[39–41] When compared to the results of Kar and Choudhary,[16] the dielectric constant of the A-K HT is higher. At 300 K and for a frequency of 10 KHz, Kar and Choudhary[16] obtained $\varepsilon' = 44$, while for our A-K treated sample, $\varepsilon' = 87$ (Table III).

The frequency variation of the loss tangent ($\tan\delta$), at 300 K, can be seen in Figure 9. Samples A-Na and A-Li have lower loss tangent, while sample A-K although presenting relatively high ε' for glass materials also possesses significant losses especially for frequencies below 10 KHz. At 10 kHz and 300 K, $\tan\delta = 0.51$ for sample A-K heat-treated (Table III), while for the ceramics prepared in Ref. 16 the loss tangent is 0.07.

As seen in Figure 9, the heat-treated A-K sample reveals a dielectric relaxation centered at about 630 Hz, which is related with electrode polarization or interfacial polarization effects. Since both, A-Na and A-Li glass ceramics, present more than one type of crystallites (Figure 1), a higher number of interfacial dipoles with different response times are expected. Therefore, their dielectric relaxation time should be higher than the one detected in the A-K glass ceramic, and their relaxation might be detected only at frequencies below the minimum range of the equipment.

Figure 10 depicts the trend of the dielectric constant and loss tangent values (Table III) of both as-grown and heat-treated glasses, at 300 K and 10 kHz. For the as-grown samples, $\tan\delta$ decreases with the increase of the alkali ion mass/radius.

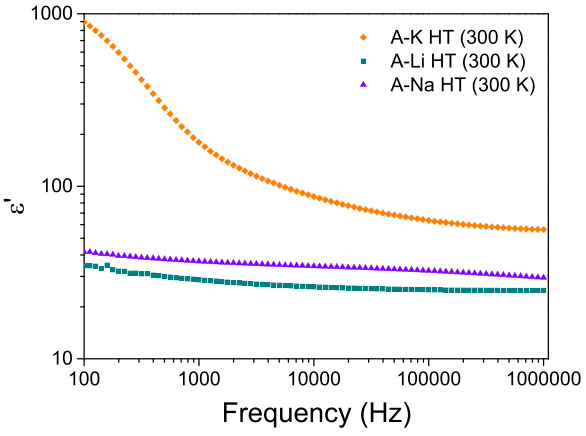

FIG. 8. Dielectric constant versus frequency, at 300 K, for the heat-treated samples (maximum uncertainty 10%).

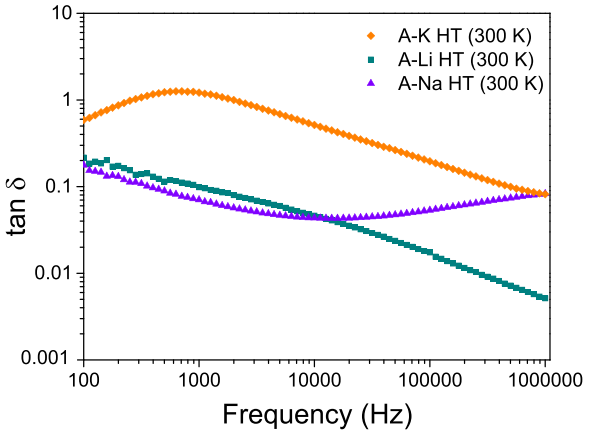

FIG. 9. Loss tangent versus frequency, at 300 K, for the heat-treated samples (maximum uncertainty 12%).

While ε' initially follows the same trend, from sample A-Na to A-K, it increases. Since these two samples did not evidenced the formation of crystalline particles, their number of electric dipoles is only related with the modifier ions in the glass matrix. Therefore, this trend could be due to an increased number, in sample A-K, of free ions structurally inserted in the glass as glass-modifiers. Also, as formerly discussed, glass A-K showed a larger formation of orthoborate groups from BO_3 triangular units, isolated orthophosphate tetrahedra (Q^0), and WO_4 tetrahedra which might also contribute to the increase of ε'.

In the heat-treated samples, the dielectric constant follows a distinct behavior relatively to the as-grown samples. Initially, ε' slightly increases from sample A-Li to A-K and then a more pronounced increase from A-Na to A-K occurs. The sharp increase of ε' for sample A-K is related with the ferroelectric behavior of the crystalline phase $KNbWO_6$,[15,16] which was the only phase formed in this sample.

The loss tangent value of the glass-ceramics also presents a different behavior. Although, for heat-treated A-Li and A-Na glasses, $\tan\delta$ is practically the same, for sample A-K, it increases significantly, following the increase of this sample's dielectric constant.

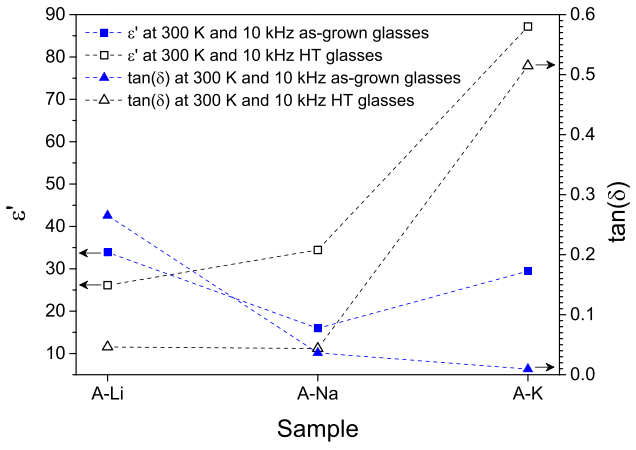

FIG. 10. Evaluation of the dielectric constant and loss tangent, at 300 K, of all samples.

Figure 10 allows to investigate the effect of the heat-treatment on each sample. For sample A-Li, ε' decreases by about 10 units, while $\tan\delta$ decreases more significantly. The decrease of the dielectric constant should be related with a superficial crystallization of the $LiNb_3O_8$ particles.[42] Generally, the amorphous phase has a lower dielectric constant when compared with a crystalline phase. Therefore, in the dielectric analysis, these two zones can be associated with a model having three serial capacitors: two related to the sample surfaces and one to the bulk material (amorphous matrix).[42] If the capacity of the surfaces, related to the ε' of $LiNb_3O_8$, is larger than the capacity of the bulk material, it becomes reasonable to consider that the bulk material defines the dielectric behavior.

For sample A-Na, the heat-treatment promotes an increase of ε', while $\tan\delta$ keeps practically the same value, which is an interesting result for charge-storage based applications. In this sample, two crystalline phases are formed, $Na_2W_4O_{13}$ and $Nb_2W_3O_{14}$, which seem to contribute to the increase of the dielectric constant. In Ref. 43, polycrystalline samples of $Na_2W_4O_{13}$ were prepared by the solid-state reaction technique. While, for sample A-Na heat-treated, $\varepsilon' = 44$ at room-temperature and 10 kHz, the samples prepared in Ref. 43 exhibited at the same frequency, values of ε' up to 1233 at higher temperatures (248 °C) and $\varepsilon' \approx 110$ at room-temperature.

Finally, sample A-K shows the most significant increase of ε'; however, $\tan\delta$ also shows a remarkable increase, making this sample not so appealing as sample A-Na heat-treated for charge-storage based applications. This sample presents however the highest conductivity values (both dc and ac), as it was mentioned before.

It should be noted that the influence of the heat-treatment in the dielectric properties of the samples was analyzed for the frequency of 10 KHz in order to avoid the spatial charge and other interfacial effects that occur at lower frequencies[41,44] (for example, Figure 8 shows the increase of ε' for sample A-K at lower frequencies). At higher frequencies, starting from about 10 KHz, the dielectric constant starts to become dominated by the bulk dielectric response.

IV. CONCLUSIONS

Phosphate-borate based glasses with molar composition $20.7P_2O_5$-$17.2Nb_2O_5$-$13.8WO_3$-$34.5A_2O$-$13.8B_2O_3$ (where A = Li, Na, and K) were prepared by melt quenching technique. The as-prepared glasses were afterwards heat-treated in air, at 800 °C during 4 h which led to the formation of glass-ceramics.

The XRD analysis showed that the heat-treatment promotes the formation of crystalline particles of $LiNb_3O_8$ and $Li_6P_4W_8O_{32}$ in the glass that contains Li_2O, $Nb_2W_3O_{14}$, and $Na_2W_4O_{13}$ in the glass that incorporates Na_2O and $KNbWO_6$ in that with K_2O.

The Raman spectroscopy analysis gave additional information. The glass-ceramic A-K showed a great number of vibrations assigned to υ_s(Nb-O) in NbO_6 octahedra and υ_s(P-O-P) in PO_4 tetrahedra. For the A-Na glass-ceramic, in addition to the latter vibrational modes, numerous vibrations related to chain type metaborate groups are present. As for the heat-treated A-Li glass, the Raman spectra also revealed the presence of stretching modes of bridging oxygen in PO_4 tetrahedra, but most of the vibrational modes of this sample are assigned to the $LiNb_3O_8$ particles.

After heat-treatment, the sample with highest dc conductivity is the glass-ceramic A-K, contrarily to the as-grown case where it was the least conductive sample. Its conductivity is predominantly ionic in the evaluated temperature range. The large increase (4 orders of magnitude) of this sample's conductivity is related to the formation of $KNbWO_6$ particles. These pyrochlore-type structures present a significantly higher spontaneous polarization in the low-temperature ferroelectric phase, and higher ionic conductivity in the high-temperature superionic state.

For the A-Li treated sample, the dc conductivity is also predominantly ionic. Although glass-ceramic A-Na exhibits a predominance of electronic conductivity for lower temperatures, above 245 K, the conductivity is ruled by the mobility of the mobile ions.

The impedance spectroscopy analysis showed that for the A-Li and A-Na glass-ceramics, ε' is practically independent of the frequency and ranges from 20 to 30 (at 10 kHz and 300 K), while for A-K heat-treated is about 87. This sharp increase of ε' is related to the ferroelectric behavior of the crystalline phase $KNbWO_6$ formed in this sample.

The evolution of $\tan\delta$ as function of the measurement frequency, at 300 K, showed that glass-ceramics A-Li and A-Na have lower loss tangent and their values are very close up to 100 kHz. On the other hand, although glass-ceramic A-K presents relatively high ε' for glass materials, it also possesses significant losses, especially for frequencies below 10 KHz.

ACKNOWLEDGMENTS

The authors are grateful to the Fundação para a Ciência e Tecnologia (FCT) for the financial support offered to this work (RECI/FIS-NAN/0183/2012 (FCOMP-01-124-FEDER-027494), and Pest-C/CTM/LA0025/2013-14).

[1]M. Karabulut, E. Melnik, R. Stefan, G. K. Marasinghe, C. S. Ray, C. R. Kurkjian, and D. E. Day, J. Non-Cryst. Solids **288**, 8 (2001).
[2]C. Srinivasa Rao, K. Upendra Kumar, P. Babu, and C. K. Jayasankar, Opt. Mater. **35**, 102 (2012).
[3]R. K. Brow, J. Non-Cryst. Solids **263–264**, 1 (2000).
[4]P. Stoch, W. Szczerba, W. Bodnar, M. Ciecinska, A. Stoch, and E. Burkel, Phys. Chem. Chem. Phys. **16**, 19917 (2014).
[5]H. Doweidar, J. Mater. Sci. **25**, 253 (1990).
[6]D. R. Uhlmann and R. R. Shaw, J. Non-Cryst. Solids **1**, 347 (1969).
[7]M. P. F. Graça, B. M. G. Melo, P. R. Prezas, M. A. Valente, F. N. A. Freire, and L. Bih, Mater. Des. **86**, 427 (2015).
[8]M. P. F. Graça and M. A. Valente, *Glass Ceramics with Para, Anti or Ferroelectric Active Phases, Advances in Ceramics - Electric and Magnetic Ceramics, Bioceramics, Ceramics and Environment* (INTECH Open Access Publisher, 2011).
[9]M. P. F. Graça, M. G. Ferreira da Silva, and M. A. Valente, J. Eur. Ceram. Soc. **28**, 1197 (2008).
[10]M. JR, *Impedance Spectroscopy: Emphasizing Solid Materials and Analysis* (John Wiley & Sons, New York, 1987).
[11]K. J. Rao, *Structural Chemistry of Glasses* (Elsevier, 2002).
[12]M. M. R. A. Lima, R. C. C. Monteiro, M. P. F. Graça, and M. G. Ferreira da Silva, J. Alloys Compd. **538**, 66 (2012).
[13]A. L. Gusev, Phys. Status Solidi A **111**, 443 (1989).

[14]G. Ohlendorf, D. Richter, J. Sauerwald, and H. Fritze, Diffus. Fundam. **8**, 6 (2008).
[15]A. V. Knyazev, M. Mączka, and N. Y. Kuznetsova, Thermochim. Acta **506**, 20 (2010).
[16]T. Kar and R. N. P. Choudhary, J. Phys. Chem. Solids **62**, 1149 (2001).
[17]D. Kasprowicz, A. Lapinski, T. Runka, A. Speghini, and M. Bettinelli, J. Alloys Compd. **478**, 30 (2009).
[18]I. Mazali, L. Barbosa, and O. Alves, J. Mater. Sci. **39**, 1987 (2004).
[19]N. Krishna Mohan, G. Sahaya Baskaran, and N. Veeraiah, Phys. Status Solidi A **203**, 2083 (2006).
[20]L. Sirleto, M. G. Donato, G. Messina, S. Santangelo, A. A. Lipovskii, D. K. Tagantsev, S. Pelli, and G. C. Righini, Appl. Phys. Lett. **94**, 031105 (2009).
[21]A. Moguš-Milanković, A. Šantić, A. Gajović, and D. E. Day, J. Non-Cryst. Solids **325**, 76 (2003).
[22]D. Boudlich, L. Bih, M. E. H. Archidi, M. Haddad, A. Yacoubi, A. Nadiri, and B. Elouadi, J. Am. Ceram. Soc. **85**, 623 (2002).
[23]R. K. Brow, D. R. Tallant, S. T. Myers, and C. C. Phifer, J. Non-Cryst. Solids **191**, 45 (1995).
[24]C. Yue, X. Zhu, M. Rigutto, and E. Hensen, Appl. Catal., B **163**, 370 (2015).
[25]C. Gejke, E. Zanghellini, J. Swenson, and L. Börjesson, J. Power Sources **119–121**, 576 (2003).
[26]L. Singh, V. Thakur, R. Punia, R. S. Kundu, and A. Singh, Solid State Sci. **37**, 64 (2014).
[27]M. P. F. Graça, M. A. Valente, and M. G. Ferreira Da Silva, J. Mater. Sci. **41**, 1137 (2006).
[28]A. Bartasyte, V. Plausinaitiene, A. Abrutis, S. Stanionyte, S. Margueron, P. Boulet, T. Kobata, Y. Uesu, and J. Gleize, J. Phys.: Condens. Matter **25**, 205901 (2013).
[29]B. P. Dwivedi and B. N. Khanna, J. Phys. Chem. Solids **56**, 39 (1995).
[30]A. A. Ahmed, N. A. Sharaf, and R. A. Condrate, Sr., J. Non-Cryst. Solids **210**, 59 (1997).
[31]S. Oishi, N. Endo, and M. Itoh, J. Cryst. Growth **229**, 477 (2001).
[32]K. Viswanathan, J. Chem. Soc., Dalton Trans. **1974**, 2170.
[33]G. P. Mohanty and L. J. Fiegel, Acta Crystallogr. **17**, 454 (1964).
[34]S. Wolf, J. Rensberg, H. Stöcker, B. Abendroth, W. Wesch, and C. Ronning, Nanotechnology **25**, 135611 (2014).
[35]J. C. Dyre, J. Appl. Phys. **64**, 2456 (1988).
[36]M. Mączka, J. H. Ko, D. Włosewicz, P. E. Tomaszewski, S. Kojima, J. Hanuza, and A. Majchrowski, Solid State Ionics **167**, 309 (2004).
[37]T. S. Chernaya, V. I. Simonov, and L. A. Muradyan, Butlletí de les Societats Catalanes de Física, Química, Matemàtiques i Tecnologia **12**, 427 (1991).
[38]F. S. Galasso, N. Kurti, and R. Smoluchowski, *Structure and Properties of Inorganic Solids: International Series of Monographs in Solid State Physics* (Elsevier Science, 2013).
[39]D. Rollik, S. Bauer, and R. Gerhard-Multhaupt, J. Appl. Phys. **85**, 3282 (1999).
[40]H. Ghamlouche, S. T. Mahmoud, and N. Qamhieh, J. Phys. D: Appl. Phys. **41**, 215303 (2008).
[41]P. Lunkenheimer, V. Bobnar, A. V. Pronin, A. I. Ritus, A. A. Volkov, and A. Loidl, Phys. Rev. B **66**, 052105 (2002).
[42]M. P. F. Graça, M. G. Ferreira da Silva, and M. A. Valente, J. Non-Cryst. Solids **351**, 2951 (2005).
[43]S. Chatterjee, P. K. Mahapatra, A. K. Singh, and R. N. P. Choudhary, J. Mater. Sci. Lett. **22**, 99 (2003).
[44]A. F. L. Almeida, P. B. A. Fechine, M. P. F. Graça, M. A. Valente, and A. S. B. Sombra, J. Mater. Sci.: Mater. Electron. **20**, 163 (2009).